ResearchGate

See discussions, stats, and author profiles for this publication at: https://www.researchgate.net/publication/357540953

Cross-continental hydroclimate proxies: Tree-rings in Central Chile reconstruct historical streamflow in Southeastern South American rivers

Article *in* Progress in Physical Geography Earth and Environment · January 2022

DOI: 10.1177/03091333211067466

CITATIONS
3

READS
502

8 authors, including:

Isabella Aguilera Betti
Pontificia Universidad Católica de Valparaíso
24 PUBLICATIONS **491** CITATIONS
SEE PROFILE

Ariel Muñoz
Pontificia Universidad Católica de Valparaíso
86 PUBLICATIONS **1,215** CITATIONS
SEE PROFILE

Paulina Puchi
Italian National Research Council
22 PUBLICATIONS **150** CITATIONS
SEE PROFILE

Gonzalo Sapriza-Azuri
Universidad de la República de Uruguay
32 PUBLICATIONS **493** CITATIONS
SEE PROFILE

All content following this page was uploaded by Ludmila Profumo on 11 January 2022.

The user has requested enhancement of the downloaded file.

Check for updates

Main Article

Cross-continental hydroclimate proxies: Tree-rings in Central Chile reconstruct historical streamflow in Southeastern South American rivers

Progress in Physical Geography
2022, Vol. 0(0) 1–23
© The Author(s) 2022
Article reuse guidelines:
sagepub.com/journals-permissions
DOI: 10.1177/03091333211067466
journals.sagepub.com/home/ppg
SAGE

Christine Lucas
Laboratorio Ecología Fluvial, Departamento del Agua, Centro Universitario Regional Litoral Norte, Universidad de la República, Paysandú, Uruguay

Isabella Aguilera-Betti
Laboratorio de Dendrocronología y Estudios Ambientales, Instituto de Geografía, Pontificia Universidad Católica de Valparaíso, Valparaíso, Chile; Centro Transdisciplinario de Estudios Ambientales y Desarrollo Humano Sostenible (CEAM), Universidad Austral de Chile, Valdivia, Chile; and Programa de Doctorado en Ciencias Antárticas y Subantárticas, Universidad de Magallanes, Punta Arenas, Chile

Ariel A Muñoz
Laboratorio de Dendrocronología y Estudios Ambientales, Instituto de Geografía, Pontificia Universidad Católica de Valparaíso, Valparaíso, Chile; Centro de Acción Climática, Pontificia Universidad Católica de Valparaíso, Valparaíso, Chile; and Centro de Ciencia del Clima y la Resiliencia CR2, Santiago, Chile

Paulina Puchi
Dipartimento Territorio e Sistemi Agro-Forestali (TESAF), Universitá degli Studi di Padova, Padova, Italia

Gonzalo Sapriza
Laboratorio Ecología Fluvial, Departamento del Agua, Centro Universitario Regional Litoral Norte, Universidad de la República, Paysandú, Uruguay

Ludmila Profumo
PDU Sistemas Territoriales Complejos, Centro Universitario de Rivera, Universidad de la República, Uruguay

R Stockton Maxwell
Department of Geospatial Science, Radford University, Radford, Virginia, USA

Alejandro Venegas-González
Hémera Centro de Observación de la Tierra, Escuela de Ingeniería Forestal, Facultad de Ciencias, Universidad Mayor, Chile

Corresponding author:
Christine Lucas, Laboratorio Ecología Fluvial, Departamento del Agua, Centro Universitario Regional Litoral Norte, Universidad de la República, km 363 Ruta 3, EEMAC, Paysandú, 60000, Uruguay.
Email: clucas@cup.edu.uy

Abstract

Regional teleconnections permit cross-continental modeling of hydroclimate throughout the world. Tree-rings are a good hydroclimatic proxy used to reconstruct drought and streamflow in regions that respond to common global forcings. We used a multi-species dataset of 32 tree-ring width chronologies from Chile and Uruguay as a climate proxy to infer annual streamflow (Q) variability in the Negro River basin, a grassland-dominated watershed of lowland Southeastern South America. A positive linear correlation between tree-ring chronologies from Central Chile and annual Negro River instrumental streamflow from 1957 to 2012 indicated a cross-continental teleconnection between hydroclimate variability in Central Chile and Northeastern Uruguay. This relationship was mediated in part by the El Niño Southern Oscillation (ENSO), whereby the El Nino 3.4 Index was positively correlated with regional rainfall, annual tree growth, and Q anomalies. Despite the proximity of Uruguayan tree-ring chronologies to Negro River hydrometric stations, the Chilean tree-ring chronologies best predicted annual streamflow. Thus, using tree-ring data from four long-term moisture-sensitive chronologies of the species *Cryptocarya alba* in Central Chile (32–34°S), we present the first streamflow reconstruction (1890–2009) in the lower La Plata Basin. The reconstruction supports regional evidence for increasing frequency of extreme flood years over the past century in Uruguay. We demonstrate how climate teleconnections that mediate local hydroclimate variability permit the cross-continental reconstruction of streamflow, filling a major geographical gap in historical proxies for flooding and drought in grassland biomes of the southern hemisphere.

Keywords

Dendrohydrology, El Niño, La Plata River, Southeastern South America, teleconnection, Uruguay

I. Introduction

River ecosystems in Southeastern South America (SESA) sustain one of the world's most important agricultural regions, as well as a series of hydroelectric dams that supply power to some of South America's most populated areas (Barros et al., 2005). Water management and flood control are a central focus in SESA given the reliance on rivers for hydropower, water supply, and agriculture (Cuya et al., 2013). The conversion of natural grasslands to intensive agriculture and afforestation within the region (Baldi and Paruelo, 2008; Modernel et al., 2016; Vega et al., 2009) has resulted in changes in evapotranspiration rates and streamflow (Lee and Berbery 2012; Silveira et al. 2016). While increasing precipitation and more severe flooding events are expected under climate change scenarios for the Southeastern Rio de La Plata Basin (RPB) (IPCC, 2021), land-use conversion and agricultural intensification place increasing demands on water resources (Barros et al., 2005). These pressures on water resources in SESA make understanding the dynamics of river systems a critical part of resource management and planning for sustainable development. Given the relatively short-term instrumental records (Doyle and Barros, 2011), there is a need for long-term data on historical streamflow for water management and climate risk assessments. Moreover, hydro-meteorological extremes are shown to be non-stationary, featuring trends and shifts (IPCC, 2014) not adequately represented by short-term datasets (Williams et al., 2021).

Tree-ring networks are used to reconstruct annual and seasonal hydroclimate variability in broad geographical regions (Coulthard et al., 2021; Higgins et al., 2020; Meko and Woodhouse, 2011; Sauchyn et al., 2011; Maxwell et al., 2017). While Southern Annular Mode (SAM) influences tree growth throughout the extra-tropical Southern Hemisphere (Villalba et al., 2012), El Niño Southern Oscillation (ENSO) plays a critical role for growth, precipitation and streamflow anomalies in tropical and subtropical latitudes (Garreaud, 2009). The relative scarcity of trees in SESA grasslands (Bogino and Jobbágy, 2011; Oliveira et al., 2010) places a regional challenge for tree-ring reconstruction of hydroclimate. The few chronologies available in lowland SESA capture a

regional signal in rainfall variability (Lucas et al., 2018), suggesting their potential as streamflow proxies. In this context, some studies show that streamflow reconstruction is improved by incorporating tree-ring chronologies from a broader spatial footprint, based on regional teleconnections to global climate factors including ENSO (Allen et al., 2013; Muñoz et al., 2016). The South American Drought Atlas (SADA) reconstructs over 600 years of austral summer drought for southern South America, drawing upon 283 tree-ring chronologies in largely high-elevation regions (Morales et al., 2020). Streamflow reconstruction of the Neuquén River in Argentina was developed based on 66 precipitation-sensitive tree-ring chronologies extending over 800 km from 32 to 44°S (Mundo et al., 2012). In the Murray–Darling basin of South-Eastern Australia, proxy records from tree-rings and coral in Indonesia, Asia, and Australia were used to reconstruct river streamflow (Gallant and Gergis, 2011). Pulling proxy data from a broader area in Australasia was a strategy to increase predictors tied to large-scale global climate forcings such as ENSO and SAM (Allan, 1988). Among the few streamflow reconstructions in the RPB, is the reconstruction of over 300 years of dry-season streamflow of the Rio Bermejo in the Chaco region (Ferrero et al., 2015). Most of the older tree-ring chronologies in SA are from Chile and Argentina, which constitute the main database for most of the climate reconstructions in SA (Christie et al., 2011; Garreaud et al., 2017; Muñoz et al., 2020; Lara et al., 2020; Aguilera-Betti et al., 2017).

ENSO variability is a key driver of hydroclimate in SESA and central Chile (Garreaud et al., 2009; Penalba and Rivera, 2016; Grimm et al., 2000). The ENSO influence on extreme seasonal precipitation events has resulted in some of the largest flooding events in the La Plata Basin (Grimm and Tedeschi, 2009). In the southeastern RPB, the Uruguay River displays streamflow anomalies that correlate positively with the El Niño 3.4 Index (Genta et al., 1998; Robertson and Mechoso, 1998). The influence of ENSO on seasonal precipitation in SESA is seasonal, whereby the ENSO signal is strongest in Oct–Dec and Mar–Jul and effectively disappears in mid-summer (Jan–Feb) (Cazes-Boezio et al., 2003; Grimm et al., 2000). Understanding the relationship between ENSO and the Uruguay River has shed insight on increasing trends in discharge since the 1960s (Pasquini and Depetris, 2007), and increasing extreme flood events (Camilloni et al., 2013; Cavalcanti et al., 2015). The Negro River is the largest tributary to the Uruguay River and likewise has a positive correlation with ENSO (Talento and Terra, 2013). ENSO and other climate forcings also influence water availability in central Chile, currently undergoing a megadrought with reductions of 20–40% in precipitation (Garreaud et al., 2017, 2020). There is a strong positive influence of El Niño on precipitation in central Chile (Garreaud, 2009), both of which influence annual tree-ring growth (Barichivich et al., 2009; Le Quesne et al., 2006, 2009; Venegas-González et al., 2018).

Tree-ring chronologies in the Southern Hemisphere share common climate signals including ENSO and SAM (Morales et al., 2020; Villalba et al., 2012). Considering the strong link between these climate modes and local rainfall in Uruguay and Central Chile (Cazes-Boezio et al., 2003; Chiew and McMAHON, 2002; Garreaud et al., 2009; Penalba and Rivera, 2016; Pisciottano et al., 1994), we evaluated cross-continental proxy tree-ring chronologies for historical streamflow variability in the largest river in Uruguay, the Negro River. We aimed to: (1) explore the correlations among ENSO, regional precipitation and annual tree-growth as a potential mechanism for the tree-ring correlation with streamflow; (2) reconstruct annual streamflow variability in two rivers in the Negro Basin using long-term tree-ring chronologies from Central Chile. We focused the analysis on how regional hydroclimate anomalies in the grasslands of humid subtropical Uruguay are connected to those in semi-arid Central Chile, and how longer-term chronologies in Central Chilean forests track Negro River streamflow anomalies in comparison to short-term chronologies from the sparsely forested landscape in the northern Pampa biome of Southeastern South America (Toranza et al., 2019). We aim to advance knowledge on historical streamflow of major rivers in Southeastern South America, using longer time series data from a network of tele-connected sites in South America.

II Materials and methods

2.1 Negro River basin streamflow. The Negro River covers approximately 69,700 km^2, 77% of which

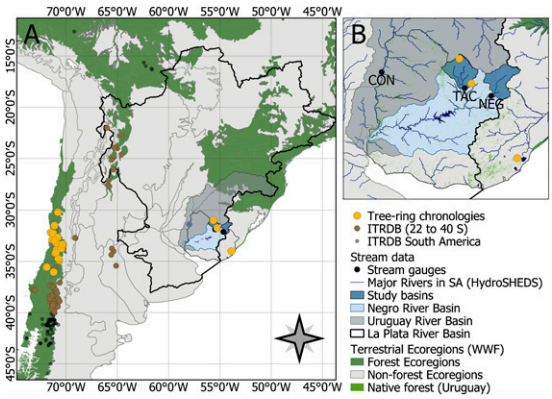

Figure 1. Map of the study area, showing (a) location of tree ring chronologies (N = 32) and ITRDB chronologies, WWF forest and non-forest biomes, and major rivers (Lehner et al., 2008) as a reference; and (b) map of the Negro River basin within the Uruguay River basin, showing the two hydrometric stations (TAC: Tacuarembó R.—Borracho Pass; NEG: Negro R.—Mazangano Pass) and respective sub-basins. Historical Q data was also used as a reference from the Uruguay River—Concordia Station (CON). Native forest cover in Uruguay (Sentinel imagery data, MGAP, 2018) shows the limited extent of native forest within this region of the Pampa biome. For interpretation of the references to colours in this figure legend, refer to the online version of this article.

ocurrs in Uruguay and a small headwater region in Southern Brazil (Figure 1). The river is the largest tributary of the Uruguay River with a length of 560 km and a mean annual discharge of 500 $m^3\ s^{-1}$ (Krepper et al., 2003). Monthly streamflow (Q) in the Upper Negro River basin declines in summer, with < 30% of annual accumulated Q occurring in Dec–Mar (Figure 2(b)). Low-flow events occur in months with the highest temperatures (Feb-1965 and 1979; Jan-1989, 1990, and 2012), but high-flow events occur throughout the year, with the highest on record as April 1959. The Negro River has three hydroelectric dams, creating three man-made reservoirs, constructed in *ca.* 1948, 1960, and 1982, the largest of which—Rincon del Bonete—has an area of *ca.* 1100 km^2. There are 28 active gauges in the basin, including on the Tacuarembó River, which covers 20% of the Negro River basin (Figure 1), The earliest water level readings are from 1911 at the San Gregorio station (García and Vargas, 1998). We obtained monthly Q data from six gauge stations upstream of all dams from the Negro, Tacuarembó, Cuñapirú, and Yaguarí Rivers, all within the Upper Negro R. basin (DINAGUA, 2018: , unpubl. data, Supplemental Table S1). Missing data (2–3%) was filled by developing an Autoregressive Integrated Moving Average (ARIMA) model with

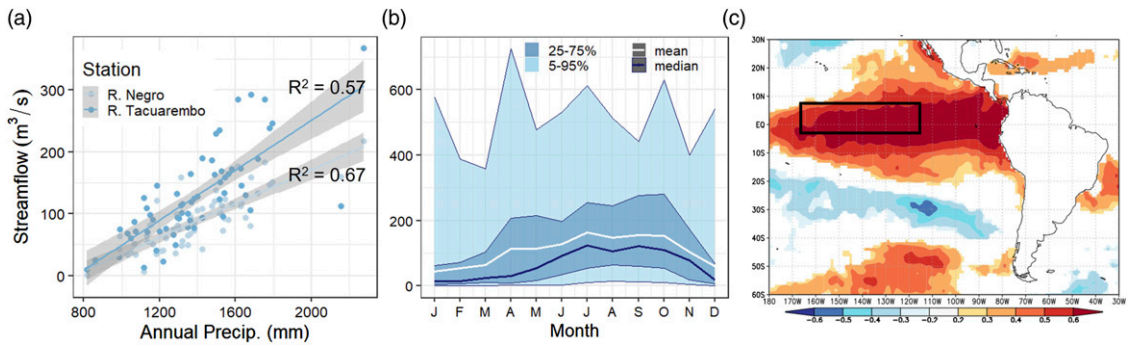

Figure 2. (a) Linear regression of mean annual precipitation and mean annual streamflow for each hydrometric station, Negro River (Adj R^2 = 0.67, p<0.001) and Tacuarembó River (Adj R^2 = 0.57, p < 0.001); (b) monthly streamflow (Q) averaged between the two stations from 1957 to 2012. Percentiles of monthly filled Q shown as shaded areas, whereby the area in light gray = 5–95% and in gray = 25–75%. Mean Q is shown as a white line and mode as a blue line. (c) Map of the correlation (r-value, p < 0.10) between 5-month averaged mean Q (Oct–Feb) and sea surface temperature (Nov–Mar), outlining in black the El Nino 3.4 region. For interpretation of the references to colours in this figure legend, refer to the online version of this article.

exogenous variables (Tencaliec et al., 2015). Correlations among six hydrometric stations prior to filling of missing data ranged from $r = 0.84$ to 0.99 ($p < 0.001$). The ARIMA captured the temporal structure of the time series; the exogenous variables (other gauge stations) took into account the correlation between gauge stations (Supplementary Figures S1 & S2).

Monthly Q (1957–2012) and average Q for two stations, Tacuarembó River—Borracho Pass (TAC) and the Negro River—Mazangano Pass (NEG), were used for all Q analyses (Table 1). A weighted mean was not used as basins were both approximately 6600 km^2 (Table 1). Both stations were located > 100 km upstream from large dams (Figure 1). We used linear regression to test the relationship between annual Q and annual precipitation for each basin (Figure 2(a)). We used the hydrostats package version 0.2.6 (Bond, 2018) in R to evaluate high and low-flow events and duration for 5th and 95th percentile Q (Figure 2(b)). Given the aseasonality of flooding events in these watersheds, we analyzed the Q–tree-ring relationship over 12-month periods.

2.2 Tree-ring data

We compiled a dataset of 32 ring width chronologies from the Southern Cone in regions influenced by ENSO (Figure 3(c) and (d) that overlapped the 55-year instrumental Q data time series from 1957 to 2012, 29 from Chile and three from Uruguay (Table 2 and Figure 1). Details regarding the collection of tree-ring samples in Uruguay and data processing are detailed in Lucas et al. (2018) for ICR and SLB, and unpublished chronology VAR was developed using similar methods. The 29 tree-ring chronologies from 10 species of Central Chile (30–36° S; Table 2) were obtained from the Laboratory of Dendrochronology and Environmental Studies at the Pontifical Catholic University of Valparaiso (PUCV) and Dendroecology Lab at the Universidad Mayor (UMayor), some of which were published (Matskovsky et al., 2021; Venegas-González et al., 2018) and others were unpublished data. Tree-ring chronologies were developed using conventional dendrochronological procedures (Speer, 2010), including wood drying and sanding with progressively finer sandpaper from 100–800 grains cm^2. The computer program COFECHA was used to detect measurement and cross-dating errors (Holmes, 1983). All chronologies were detrended using a cubic smoothing spline two-thirds the length of the series (Speer, 2010). The Expressed Population Signal statistic (EPS; Briffa, 1995) was used to assess the strength of the common growth signal over time and truncate the chronologies when this signal weakens in the less replicated, earlier part of the chronology. We retained for analysis segments of the Chilean chronologies with EPS above the commonly used threshold of 0.85 (85% common growth signal and 15% noise) and UY chronologies >0.80 (Lucas et al., 2018).

We developed three composite chronologies based on Principal Component Analysis (PCA) of chronologies from central Chile in order to identify the common growth pattern variability among the site chronologies. The first PCA (PCA-Q) was based on $N = 21$ chronologies that correlated with mean annual Q (Jun–May); we used PC1 to compare with Q and precipitation over the instrumental period 1957–2012 (Supplementary Figure S3). We developed a second PCA (PCA-ENSO) based on the $N = 16$ chronologies that correlated with 5-month averaged ENSO (May–Sep), to compare with El Niño 3.4 Index (Supplementary Figure S4). A third PCA (PCA-100) was conducted based on $N = 18$ chronologies that extended over a century (1906–2011) to examine long-term correlation with ENSO and

Table 1. Gauge stations evaluated in this study, indicating mean monthly streamflow (Q) and Mean Streamflow (Mean Q) between the two stations. Number of months with missing data in the entire series are indicated.

Gauge station	Period	Area (km^2)	Missing data	Outlet altitude (m)	Q mean ± SD (m^3/s)
Río Negro—Mazangano	1957–2012	6578	22	104	89 ± 101
Río Tacuarembó—Borracho	1955–2012	6589	19	97	129 ± 153
Mean Q	1957–2012	NA	-	-	109 ± 123

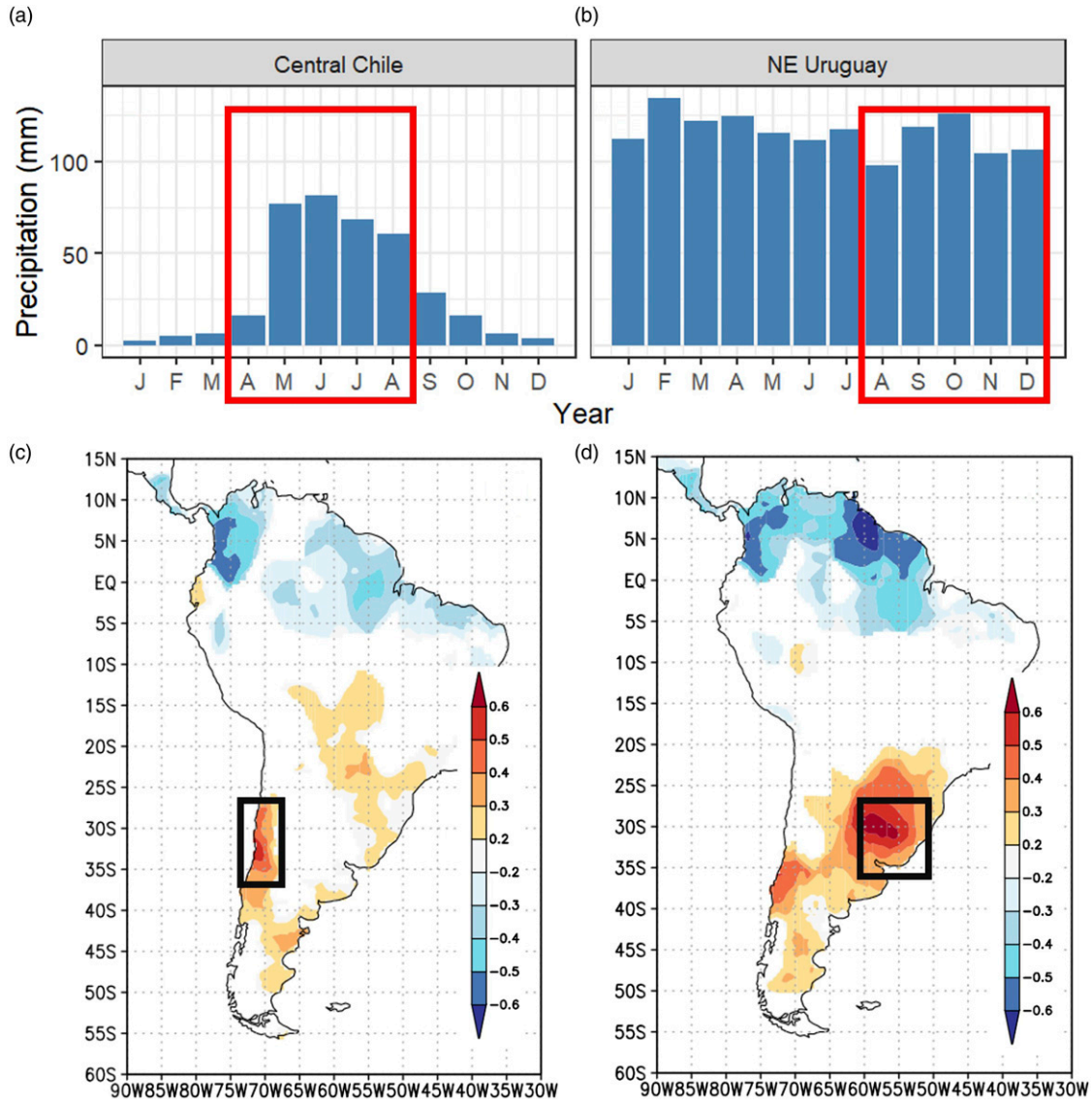

Figure 3. Mean monthly precipitation in (a) Central Chile and (b) NE Uruguay from 1957 to 2012 Map of the spatial correlation (r, $p < 0{,}10$) between (c) 5-month averaged Apr–Aug rainfall and the El Nino 3.4 Index and d) Aug–Dec rainfall and El Nino 3.4 Index; Sep–Dec in South America, developed in KNMI Climate Explorer. For interpretation of the references to colours in this figure legend, refer to the online version of this article.

regional precipitation in central Chile (Supplementary Figure S5).

2.3 Climate data

Regional rainfall. Central Chile and Uruguay have dramatically different rainfall regimes (Figure 3(a) and (b), which affect the timing and strength of the relationship between tree-ring growth and Q. Monthly rainfall in NE Uruguay and Central Chile from 1901 to 2017 were obtained from the 0.5° CRU 4.03 dataset (Harris et al., 2020). The climate in Uruguay is characterized as humid subtropical (*Cfa*)

Table 2. Tree-ring width chronologies from Chile and Uruguay evaluated as potential proxies for streamflow (Q) of the Upper Negro River from 1957 to 2012. Chronologies are ordered from north to south (latitude = Lat), showing interseries correlation (*r*), total number of series (N°), as well as correlation (*r*) with 5-month averaged ENSO (May–Sep in Chile; previous (p) Oct–Feb in Uruguay, precipitation (PPT) in Central Chile (May–Sep) or Uruguay (pNov–Mar), and annual Q (Jun–May in Chile; pSep–Aug in Uruguay). Chronologies in bold (*n* = 7) were used to evaluate various reconstruction models, and *n* = 4 sites with an asterisk were selected for final models.

Code	Site	Elevation (masl)	Species	Lat	Period	Series *r*	N° series	N° trees	*r* ENSO	*r* PPT	*r* Q
Chile									May–Sep	May–Sep	Jun–May
TOL	Tololo sitio 1	1780	*PrCu*	−30.19	1691–2013	0.63	37	13	**0.35**	**0.55**	**0.28**
CHI	Chinchillas	1488	*AcCa*	−31.5	1917–2016	0.41	24	14	0.13	0.05	0.16
INE	Cerro Santa Inés	641	*AePu*	−32.16	1780–2016	0.41	25	18	0.11	−0.14	0.09
CSI**	Cerro Santa Inés	227	*CrAl*	−32.17	1749–2017	0.48	39	26	**0.33**	**0.44**	**0.27**
PML*	Maitén Largo	188	*CrAl*	−32.26	1890–2017	0.82	29	16	**0.30**	**0.60**	**0.50**
BML	Maitén Largo	190	*BeMi*	−32.26	1790–2017	0.56	21	16	**0.32**	**0.53**	**0.37**
ELA	El Asiento	1878	*AuCh*	−32.65	1153–2017	0.69	47	32	**0.22**	**0.68**	**0.36**
BQ	El Manzanar	280	*BeMi*	−32.89	1927–2017	0.68	42	34	**0.32**	**0.69**	**0.35**
CAM	PN La Campana	1257	*NoMa*	−32.96	1905–2017	0.63	79	46	0.19	**0.50**	**0.27**
RLC	PN La Campana	1329	*NoMa*	−32.96	1904–2014	0.6	47	29	**0.31**	**0.59**	**0.37**
CER	Cerro El Roble	1964	*NoMa*	−32.99	1910–2016	0.52	42	25	***0.19***	**0.41**	**0.23**
PLC	PN La Campana	400	*CrAl*	−33	1891–2017	0.75	21	15	**0.24**	**0.71**	**0.47**
BLC	PN La Campana	623	*BeMi*	−33	1913–2017	0.7	18	11	0.16	**0.64**	**0.43**
ACH	Altos Chicauma	1315	*NoMa*	−33.2	1923–2018	0.7	32	24	**0.28**	**0.67**	**0.42**
PYL	Yerba Loca	2071	*KaAn*	−33.33	1936–2015	0.71	15	14	0.13	**0.47**	**0.41**
MET	Yerba Loca	2100	*KaAn*	−33.33	1876–2015	0.62	15	14	**0.23**	**0.63**	**0.44**
MAN	Manquehue	1084	*CrAl*	−33.36	1932–2015	0.65	33	18	−0.01	0.00	−0.04
SVI	Sendero del Viento	2087	*KaAn*	−33.36	1945–2016	0.54	19	13	0.16	**0.50**	**0.38**
VNE	Valle Nevado	2468	*BeAn*	−33.37	1937–2016	0.46	28	27	0.04	0.19	0.21
ADR	Aguas de Ramón	1152	*CrAl*	−33.44	1850–2011	0.63	25	15	**0.29**	**0.74**	**0.36**
PRC*	Río Clarillo	1002	*CrAl*	−33.73	1863–2017	0.65	26	13	**0.38**	**0.65**	**0.47**
PPI*	Pirque	837	*CrAl*	−33.75	1881–2018	0.73	52	26	−0.10	0.03	**0.27**
SAC	Altos Cantillana	1900	*NoMa*	−33.87	1789–2014	0.51	46	25	0.16	**0.37**	**0.24**
RNL	RN Loncha	1050	*NoMa*	−34.14	1858–2014	0.47	37	24	**0.33**	**0.37**	**0.38**
HPL	Poqui límite cumbre	1250	*NoGl*	−34.19	1733–2018	0.6	35	20	**0.32**	**0.38**	0.21
TIN	Tinguiririca	678	*CrAl*	−34.73	1942–2018	0.65	35	19	0.13	0.13	0.13
SAH	Alto Huemul	1670	*NoMa*	−34.88	1767–2014	0.47	56	39	0.15	**0.31**	0.18
PSJ	San Javier	129	*CrAl*	−35.56	1921–2018	0.61	34	18	**0.23**	**0.49**	**0.41**
ANI	Las Ánimas	968	*AuCh*	−36.04	1884–2017	0.59	32	17	***0.22***	0.05	0.09

(continued)

Table 2. (continued)

Code	Site	Elevation (masl)	Species	Lat	Period	Series *r*	N° series	N° trees	*r* ENSO	*r* PPT	*r* Q
Uruguay									pOct–Feb	pNov–Mar	pSep–Aug
VAR	Paso Vargas	188	*SeCo*	−30.98	1967–2007	0.45	24	17	0.05	**0.32**	**0.25**
ICR[b]	Isla Cristalina	200	*ScBu*	−31.73	1919–2012	0.43	29	15	**0.42**	**0.55**	**0.40**
SLB[b]	Sierra La Blanqueada	150	*ScBu*	−33.99	1900–2012	0.42	25	14	**0.28**	0.20	0.16

Note: Species scientific names and codes are as follows: *Proustia cuneifolia (PrCu), Acacia caven (AcCa), Aextoxicon punctatum (AePu), Cryptocarya alba (CrAl), Beilschmiedia miersii (BeMi), Austrocedrus chilensis (AuCh), Nothofagus macrocarpa (NoMa), Kageneckia angustifolia (KaAn), Berberis andina (BeAn), and Nothofagus glauca (NoGl).*

[a]Chronologies included in the manuscript under review in *Ecosystems*: Venegas-González A., Muñoz A.A., Carpintero-Gibson S.I, González-Reyes A., Schneider I., Gipolou-Zuñiga T., Aguilera-Betti I., and Roig F.A. Sclerophyllous forest tree growth under the influence of a historic megadrought in the Mediterranean ecoregion of Chile.

[b]Chronologies published in Lucas et al. (2018).

(Rubel and Kottek, 2010) with a mean annual precipitation (MAP) of 1398 mm y^{-1} in the study region and seasonal rainfall distributed year-round, averaging 92–121 mm mo^{-1} (Figure 3(b)). The climate in Central Chile (29–40° S), is Mediterranean (*Csa* and *Csb*) (Rubel and Kottek, 2010), highly seasonal, with a North-South gradient in MAP from 50 to 300 mm y^{-1}, where 90% of rainfall occurs in May–Aug (Barichivich et al., 2009; Garreaud et al., 2020). Above-average precipitation in rainiest months is linked to El Niño episodes, due to an increase in sea surface temperature in the equatorial Pacific regions and a decrease in atmospheric pressure (Garreaud et al., 2009; Montecinos and Aceituno, 2003). This atmospheric condition increases the frequency of frontal cloud bands and intensifies them, generating increased precipitation in Central Chile (Meza, 2013). Monthly rainfall in Uruguay was averaged among eight CRU grid points in the Upper Negro River basin, and in Central Chile, among all CRU gridded data points within the area 29–36° S and 70–71°W using the KMNI Climate Explorer (Trouet and Van Oldenborgh, 2013). As 85% of precipitation in Central Chile from 29-36°S occurs in May–Sep (Figure 3(a)), seasonal hydroclimatic variables in Chile incorporated austral winter anomalies. We used a double mass curve to compare the consistency of the relationship between CRU 4.03 annual precipitation in Central Chile and NE Uruguay rainfall in the period Jan–Dec from 1901 to 2017 (Supplementary Figure S6). Seasons were defined as Spring = Sep–Nov, Summer = Dec–Feb, Fall = Mar–May, and Winter = Jun–Aug.

Global climate data. The monthly ENSO index, ESRL/NOAA Niño 3.4, based on HadISST for 1901–2017 was downloaded from climatedataguide.ucar.edu (Schneider et al., 2013), as the best El Niño Index for explaining seasonal and annual drought anomalies (Penalba and Rivera, 2016). We used a 5-month moving average to evaluate the relationship between ENSO and tree-ring data, based on definitions of ENSO events by Trenberth (1997). The monthly SAM Index was obtained from the NCAR-UCAR Climate Data Guide (Marshall, 2003) to evaluate the correlation between Central Chile tree-ring chronologies and SAM across multiple time windows (for R values with ICR and SLB chronologies from Uruguay see (Lucas et al., 2018). Monthly data for the CSIC Standardized Precipitation Drought Index, SPEI (Vicente-Serrano et al., 2010) were obtained via the KNMI Climate Explorer (Trouet and Van Oldenborgh, 2013).

2.4 Tree-ring versus hydroclimate analyses

Tree-ring chronologies in northeastern Uruguay (UY) and Central Chile (CCh) were expected to correlate with Q over different months, given differences in rainfall seasonality (Figure 3(a) and (b)). We evaluated potential Q proxies based on the correlation between tree-ring chronologies and a seasonal ENSO signal, as

a driver of local hydroclimate. The seasonality of the relationships among tree-ring width, ENSO and Q was evaluated by exploring multiple correlations with Pearson correlation coefficients over multiple 5 and 12-month time windows. First, we evaluated the timing and strength of the relationship between Q and the ESRL/NOAA Niño 3.4 Index. Under the hypothesis that precipitation variability explains the ENSO - tree-growth correlation in both CCh and UY (Barichivich et al., 2009; Lucas et al., 2018), we mapped the correlation between Q and mean annual precipitation (Figures 3(c) and (d)). Spatial correlation maps were constructed in the Climate Explorer web analysis platform of the Royal Netherlands Meteorological Institute (KNMI: https://climexp.knmi.nl/start.cgi).

To evaluate the Q and tree-ring width correlation over monthly, seasonal and annual time scales, we applied multiple Pearson correlation coefficient analyses for the instrumental data period 1957–2012. We identified the months (static time window) with the highest correlation between tree-ring width and a 32-month climate period from January of the calendar year 2 years prior to growth onset to August of the current year (Biondi and Waikul, 2004; Blasing et al., 1984). Temporal stability of the growth-monthly streamflow relationship was assessed using a 30-year moving window beginning in 1957 and shifted forward 1 year at a time using the package treeclim (Zang and Biondi, 2015). We used multiple Pearson correlations to determine the 5 and 12-month period of consecutive months with the highest correlation to each chronology. This method accounted for the potential lag in the correlation between streamflow and tree growth (Fritts, 1976). Confidence intervals for both static and moving correlation coefficients were estimated with 1000 bootstrapped estimates obtained by random extraction with replacement from the input dataset. Wavelet analysis was used to assess periodic signals in precipitation, Q, and tree-ring data (Bunn, 2008). All analyses were conducted in R version 3.5.3 (R Core Team, 2019).

2.5. Cross-continental streamflow reconstruction

A streamflow reconstruction was evaluated based on the established teleconnection between the hydroclimates of Central Chile and NE Uruguay. Annual streamflow (previous Jun–May) of the Negro and Tacuarembó Rivers was reconstructed with tree-ring records from Chile using a multiple regression model. The chronologies selected for the model were those that extended more than 100 years, and showed positive correlations with instrumental streamflow, precipitation, and ENSO (Table 2). The common period between instrumental Q data and tree-ring chronologies (1957–2009) was used to calibrate models using a stepwise multiple linear regression following the "leave-one-out" cross-validation method (Michaelsen, 1987; Meko and Woodhouse, 2011). In this approach, each observation is successively withheld, a model is estimated on the remaining observations, and the omitted observation is predicted. Finally, the time series of predicted values assembled from the deleted observations is compared with the observed records to compute the validation statistics of accuracy and error model (Muñoz et al., 2016, 2020).

We selected potential chronologies as model parameters based on their positive correlation with both ENSO and Q (Table 2); prior to selecting the final set of parameters, a priori models with multiple species consecutively selected *Cryptocarya alba* chronologies as the strongest p. We also observed that model performance declined when adding other species. As such, we considered for Q reconstruction, seven chronologies of *C. alba,* ADR, CSI, PML, PPI, PSJ, PLC, and PRC, excluding MAN and TIN that had no correlation with any of the hydroclimate variables of interest (Table 2). The final models selected used four parameters—PML, CSI, PPI, and PRC chronologies—at year t=0, t+1, t+2, and streamflow series as predictors. The following models were selected based on the longest time series (1891–2017) with the most robust statistics

$$\mathrm{NEG} = 34.20 + 12.03\mathrm{PML}_{t=0} - 59.64\mathrm{CSI}_{t+1} + 42.32\mathrm{PRC}_{t=0} + 32.84\mathrm{PPI}_{t=0} + 21.39\mathrm{PPI}_{t=1}$$

$$\mathrm{TAC} = 32.96 + 25.75\mathrm{PML}_{t=0} - 103.55\mathrm{CSI}_{t+1} + 61.05\mathrm{PPI}_{t=0} + 46.35\mathrm{PPI}_{t+1} + 59.03\mathrm{PRC}_{t=0}$$

where NEG and TAC are the reconstructed annual streamflow for Jun–May of the Negro and Tacuarembó River, respectively. The reconstruction was truncated at 2009 due to changes in the double mass

curve of Q-precipitation post-2009 (Supplementary Figure S6), potentially related to the effects of recent increases in afforestation area in the Tacuarembó River basin in Uruguay, as well as severe growth declines in Central Chilean trees related to the megadrought in Chile in the 21st century (Venegas-González et al., 2019; Matskovsky et al., 2021).

Model verification for the calibration period (1957–2009) was conducted using the R^2 and adjusted R^2 to evaluate explained variance between observed and predicted values, the latter adjusted for loss of degrees of freedom; the F statistic for testing the accuracy of the regression model; and the reduction of error (RE) statistic to account for the relationship between the actual value and the estimate. The robustness of the reconstruction was evaluated using the root mean square error (RMSE), the Reduction Error (RE), and the Durbin–Watson test (DW) (Fernández et al., 2018; Muñoz et al., 2020). We evaluated the linear correlation between the reconstruction and historical hydroclimate data from the Upper Negro River basin, including annual CRU 4.03 precipitation, CSIC 1-month SPEI, and the annual self-calibrated Palmer Drought Severity Index (scPDSI) available at the SADA Explorer (https://sada.cr2.cl/, Morales et al., 2020). We also compared the reconstruction with the El Niño 3.4 Index from 1901 to 2017 and annual Q (Jun–May) of the Uruguay River at Concordia (31°24′S and 58°2′W) from 1898 to 2005 (unpubl. data, CTM, 2020), one of the oldest river level gauges in lower Uruguay R. basin. Finally, the periodicity of the reconstruction was evaluated by wavelet analysis using the *morlet* function in the dplR library and violin plots. A wavelet analysis on both the ENSO and reconstructed Q were used to determine if there were significant periodicities expected if ENSO was a driver of historical Q and climate in Uruguay. Frequency of extreme events (>95% and <5% exceedance) were evaluated in the hydrostats package version 0.2.6 (Bond, 2018), including a list of very wet and dry years pre- versus post-climatic jump of the 1960s in streamflow of rivers in SESA (Mechoso and Iribarren, 1992).

III Results

3.1. Tree-growth from Central Chile as indicators of streamflow. Among the 29 potential tree-ring chronologies in central Chile, 21 were positively correlated with annual Q in Uruguay (r values in Table 2). These 21 ring-width chronologies corresponded to seven species from 30 to 36° S at altitudes of 129 to 2468 masl (Table 2). Pooling these 21 chronologies into the PCA-Q, the first component (PC1, variance = 49.9%) was positively correlated with annual Q from Jun–May ($r = 0.50$, $p < 0.001$) during the same period of ring formation (approximately Sep–May) in the Southern Hemisphere (Figures 4 and 5(a)). Chronologies differed in the timing and strength of correlation with annual Q (Table 2), with variable seasonal Q signals in the previous winter, and in spring-summer of the same growth year (Table 2 and Supplementary Figure S7). Precipitation of May–Sep (5-month average) also had a strong positive correlation with PC1 ($r = 0.80$, $p < 0.001$, Figure 4), showing that increased precipitation in winter in CCh precedes increased tree growth in the following growth year. There was a strong correlation between r-values with Q and r-values with precipitation in CCh ($r = 0.64$, $p < 0.01$), showing that trees highly correlated with regional precipitation in Chile were also good predictors of annual Q in Uruguay.

Most chronologies showed a correlation with ENSO in the current growth year, but chronologies TIN, MAN and SAH shared a pattern similar to Uruguayan chronologies, with an ENSO signal one or two years prior to ring formation (Supplementary Figure S8). Among the 29 chronologies from central Chile, 16 were positively correlated with the 5-month El Niño 3.4 Index (May–Sep or Apr–Aug, $p < 0.10$), 14 of which also correlated with Q. PC1 (48% variance), based on these 16 chronologies (PCA-ENSO), was also positively correlated with the El Niño 3.4 Index across multiple 5-month time windows, the strongest of which was May–Sep ($r = 0.40$, $p = 0.001$). In contrast to ENSO, correlation with annual SAM was negative among seven chronologies ($r = -0.27$ to -0.46, $p < 0.05$, HPL, SAH, MOD, PRC, CSI, MAN, and ANI), which varied broadly in the timing of the correlation. An additional three chronologies (CHI, VNE, and TOL) had a weak positive correlation with SAM ($r < 0.32$), but the remaining 19 chronologies from Chile showed no relationship with annual SAM anomalies.

The modular effect of ENSO on tree-ring growth was shown using the PCA-100 based on 18

chronologies starting prior to 1906 (Table 2). Over a century, the correlation between ENSO and PC1 (42.1% variance) was $r = 0.38$ ($p < 0.001$), with periods of high (1906–1940, $r = 0.62$, $p < 0.001$ and 1980–2011, $r = 0.58$, $p < 0.001$) and low correlation values (1940–1980, $r = 0.14$, NS, Figure 6). Meanwhile, the correlation between central Chile precipitation and Axis 1 of the PCA-100 was high ($r = 0.73$) and consistent through time ($r = 0.69$, 0.73, and 0.78, $p < 0.001$, for 1905–1940, 1941–1975, and 1976–2012, respectively, Figure 6). Overall, results showed decadal variation in the correlation between ENSO and tree-ring width, while the correlation with precipitation and tree-ring width remained significant and positive throughout the entire study period. Wavelet analyses also showed the presence of 2–7-year periodicities in Q and PC1 of the PCA-100 from 1901 to 2012, and their inconsistency over decadal scales (Supplementary Figure S10).

3.2 Tree-growth and streamflow in SESA

Among chronologies from Uruguay, one chronology (ICR) spanned the entire instrumental Q data period, located in the highlands of the Upper Negro River basin. Tree-ring chronology in NE Uruguay (ICR) was positively correlated with annual Q in the previous growth year, prior to tree-ring formation (Sep–Aug, Table 2 and Figure 5(b)). This correlation was influenced by a seasonal correlation with Q in late summer and fall (Feb–May, $r = 0.43$, $p = 0.0013$). The relationship between tree-rings and Q was strongest in

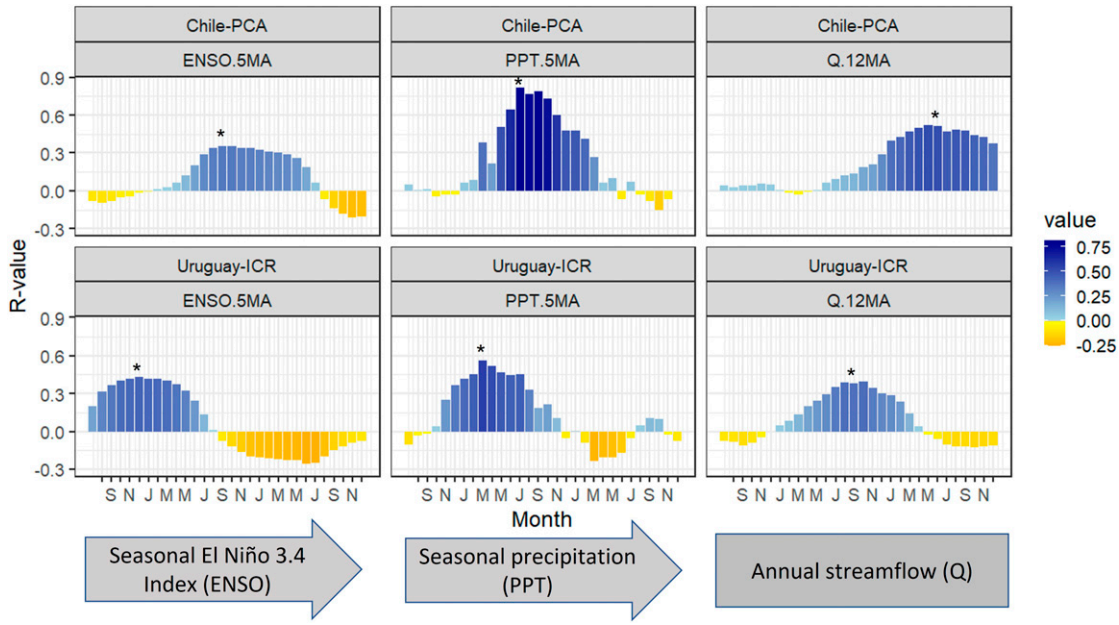

Figure 4. Pearson correlation coefficients (*r*-value) for the relationship between Axis 1 of Principal Component Analysis (PCA-Q) of 21 tree-ring width chronologies in Chile and 5-month average ENSO (El Niño 3.4 Index), 5-month average precipitation (PPT) and 12-month average streamflow (Q) from 1957 to 2012. The Sep–Aug growth year for ring formation is shown in white-filled boxes, and growth season prior to ring formation in gray along the x-axis. Asterisks indicate the 5- and 12-month periods used to analyze correlations between hydroclimate and chronologies, as shown in Figures 6 and 7, and *r* values in Table 2. For interpretation of the references to colours in this figure legend, refer to the online version of this article.

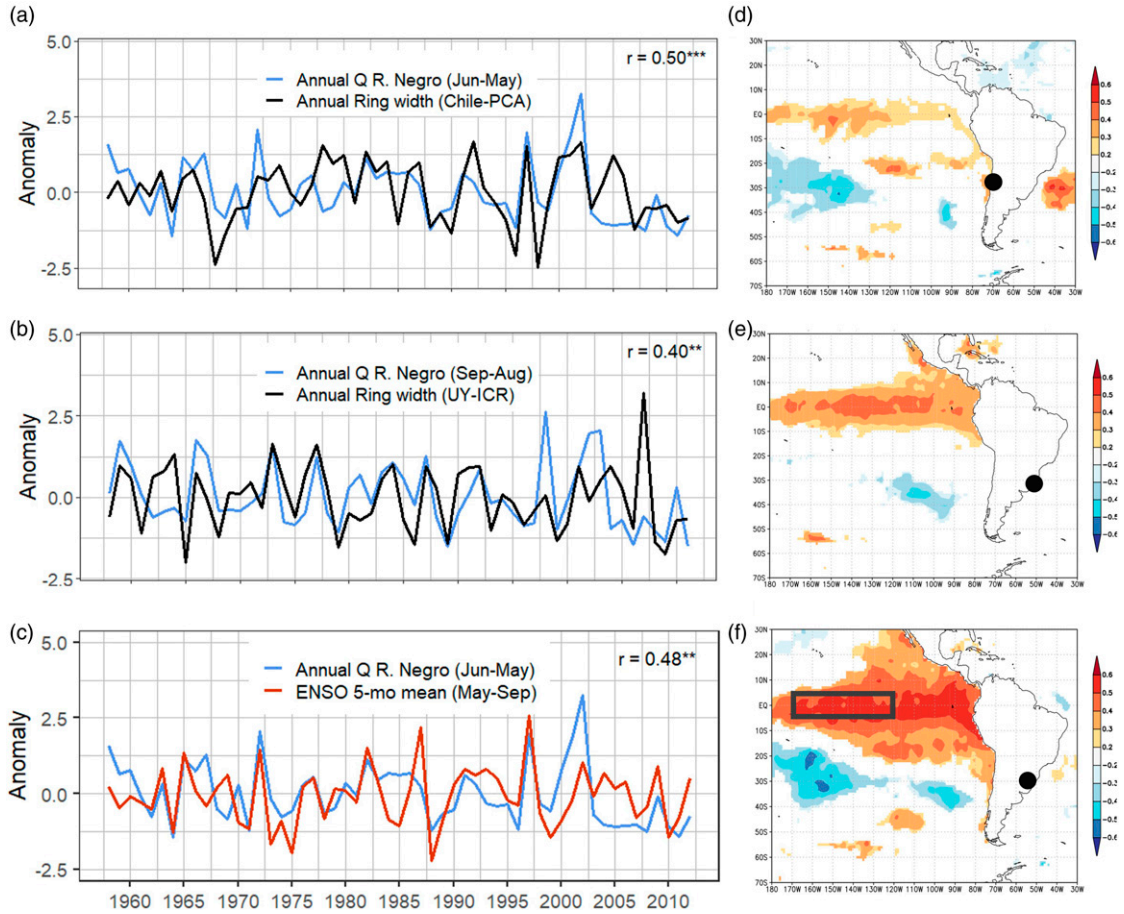

Figure 5. Time series with Pearson correlation coefficients (r) (a–c) and correlation maps ($p > 0.10$; d–f) showing interannual variability in (a,d) 5-month averaged ENSO (Aug–Dec) and annual Q (Jun–May) from 1957 to 2012. (b,e) Tree-ring anomalies from Axis 1 of Principal Component Analysis (PCA-Q) based on 21 chronologies from Chile and annual Q (Jun–May); (c,f) annual ring width chronology from Uruguay (site ICR) and annual Q (Sep–Aug), where Q is the averaged between the two gauge stations. Maps developed in the KMNI Climate Explorer; El Niño Index Region 3.4 shown as black rectangle. For interpretation of the references to colours in this figure legend, refer to the online version of this article.

March ($r = 0.41$, $p = 0.002$), and showed temporal consistency in all 35-year moving correlation windows in the 1957–2012 period ($p > 0.05$). High-flow years were registered by trees in 1966, 1973, 1977, 1984, 1987, 1998, and 2002–2003, generally following positive ENSO oscillations (Figure 5(c)). Concerning the timing of the ENSO – tree-ring connection, multiple time window correlations between UY tree-rings and hydroclimate variables, ENSO, PPT, and Q demonstrate the differences in the timing and strength of these correlations (Figure 4). In Uruguay, tree-ring growth was is positively correlated with ENSO in the 5-month period Aug–Dec, coinciding with typically peak El Niño/La Niña index values in Nov–Dec (Penalba and Rivera, 2016). Peaking slightly later, tree-ring growth was also correlated with precipitation from Nov–Mar (Figure 4), coinciding with the tail end of El Niño in Nov–Dec and hot summer temperatures in Dec–Feb (Lucas et al., 2018).

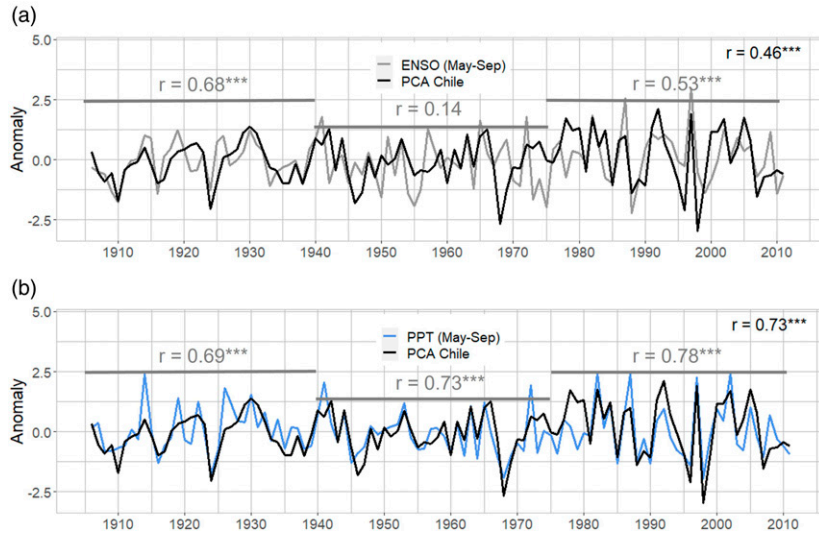

Figure 6. Time series of (a) El Nino 3.4 Index (ENSO, May–Sep) and the composite chronology from chronologies from Central Chile with overlapping data from 1904 to 2012 and (b) anomaly of annual precipitation (May–Sep) from CRU gridded data within the focal region in Central Chile. Pearson correlation coefficients (*r*) are shown for 35-year time windows over the century-long series, emphasizing the modular influence of ENSO on annual tree growth, while correlation with austral winter precipitation remains consistent over time. For interpretation of the references to colours in this figure legend, refer to the online version of this article.

Comparing all chronologies as indicators of Q in Uruguay, annual growth for most chronologies in Chile was correlated with Q in Uruguay within the same growth year, while tree-growth in Uruguay was correlated with Q in months prior to growth year. For *S. buxifolia* chronologies in SESA, annual ring width was closely tied to ENSO anomalies in the austral summer (Dec–Jan). In contrast, ring width anomalies in central Chile are closely tied to SST in the austral fall-winter (May–Aug). Given the expected time lag between ENSO anomalies, regional precipitation and mean streamflow, we found that trees in Uruguay are largely contributing to a summer-fall Q signal and trees in Chile to a complementary spring-early summer signal, both contributing to an understanding of the annual variability in Q. Wavelet analyses show varying levels of significance in the 2–4 year periodicity of Q, PPT and tree-ring data, and the weakening of this signal in the 1960s–1980s when decadal periodicities are more significant (Supplementary Figure S10).

Given that on average 85% of precipitation in central Chile occurs in May–Sep (Figure 2(a)), seasonal hydroclimatic variables in Chile incorporated austral winter anomalies. Average annual Q of the two study basins was positively correlated with the El Niño 3.4 Index ($r = 0.52$, $p < 0.01$), supporting previous studies of the Q-ENSO relationship in the Negro and Uruguay Rivers (Genta et al., 1998; Robertson and Mechoso, 1998). As the mechanism for the Q-ENSO connection is a direct relationship between local precipitation and Q, a linear relationship between annual precipitation and mean annual Q was found for both stations ($r = 0.67$, $p < 0.001$, Figure 3(a)).

3.3 Streamflow reconstruction

The 1890–2009 Q reconstruction captured 45.6% (R^2 adj = 40%) of the total variance of annual Q (Jun–May) of the Tacuarembó River (TAC) and a 40.7% (R^2adj = 34%) for the Negro River (NEG) according to R^2 values. Both reconstructions were based on four chronologies (PML, CSI, PPI, and PRC) comprising the single evergreen species *Cryptocarya alba* from sites ranging in elevation from 188 to 1002 masl and latitudes 32–34°S (Table 2). All four chronologies had

an EPS > 0.85, except for the decade 1900–1910 of PRC with an EPS of 0.81–0.84. The variance explained by the model was $R^2a = 0.40$ for TAC and $R^2a = 0.34$ for NEG (Table 3). Model skills were shown by RE = 0.33 for TAC and 0.28 for NEG. The residuals of regression models were normally distributed, and not significantly autocorrelated, according to Durbin–Watson tests DW = 1.87, 1.85 for TAC and NEG, respectively. Regarding the 1957–2005 calibration period, the correlation was $r = 0.59$ ($p < 0.001$) for TAC and $r = 0.48$ ($p < 0.001$) for NEG.

The 115-year reconstructed Q captured historical low-flow years for both rivers (<10% percentile), including in 1890, 1917–1918 (Summer PDSI -3.45 to −2.56, SADA Explorer, Morales et al., 2020), 1924, 1935, 1946, and 1996. High-flow periods (>90% percentile) were observed in the reconstructed series in 1905, 1929, 1931–1932, 1959 (including the largest flood event on record in April-1959), 1972, 1983–1984, 1997, and 2000–2002 (Figure 7). The positive correlation with the Uruguay River at Concepcion ($r = 0.40$ TAC and $r = 0.38$ NEG, Figure 7(c)) suggests that the reconstructed streamflow accurately captures part of the variability of the streamflow of the Negro and Tacuarembó Rivers in the upper basin. Correlations of the reconstructed annual Q with annual precipitation (May–Apr) were relatively strong (TAC: $r = 0.38$, $p < 0.001$; NEG: $r = 0.38$, $p < 0.001$) Meanwhile, somewhat weaker correlations were found between reconstructed Q and 1-month SPEI from Apr–Aug (TAC: $r = 0.18$, $p = 0.04$, NEG: $r = 0.20$, $p = 0.03$), SADA summer PDSI (https://sada.cr2.cl/) for Dec–Feb (TAC: $r = 0.21$, $p = 0.018$ and NEG: $r = 0.22$, $p = 0.013$) and ENSO (TAC: $r = 0.21$, $p = 0.015$, NEG: $r = 0.24$, $p = 0.007$; (Supplementary Figure S11).

The 1901–2017 ENSO records showed periodicity in the 2–7 year range, as expected, with stronger correlations in the latter part of the 20th century according to wavelet analysis (Figure 8). Reconstructed Q for TAC and NEG showed 2–5 years periodicity in more recent decades, that is 1990–2000 but not throughout the entire record. Periodicity of 5–10 years was observed in the earlier part of the century between 1910 and 1930, as well as longer-term periodicities of 16–32 years (Figure 8). In addition to the modular strength of ENSO-like periodicities in the reconstructions, violin plots showed changes in the kernel probability of reconstructed Q, with increased probability of higher annual Q post-climatic jump of the 1960s (Supplementary Material, Figure S12).

IV Discussion

The remote influences of large-scale climate oscillations on rainfall and streamflow are registered in the growth of tree-rings throughout the Southern Hemisphere (Villalba et al., 2012). Here we demonstrate that tree-ring chronologies from Central Chile and Uruguay are proxies for historical streamflow of the Upper Negro River basin in SESA. First, we demonstrate at a regional scale the positive relationship between annual tree growth and annual Q anomalies in the Negro River basin. Second, we demonstrate a relationship between annual tree growth in Central Chile and Negro River Q and show how this is influenced by a modular ENSO signal over the twentieth century. Finally, we reconstruct Negro and Tacuarembó Rivers Q using a subset of Central Chile tree-ring chronologies from 1890 to 2009. Given the limited streamflow records prior to 1960 and the relative scarcity of old-growth forests in the vast grassland biome of SESA, we show that tree-ring data from other regions in South America, linked to the same large-scale climate drivers, can improve our understanding of the long-term dynamics of these rivers that play a critical role for energy and agriculture in this productive region.

4.1 Tree-rings as indicators of historical streamflow variability

Ocean-atmosphere-land teleconnections among remote regions can permit the historical reconstruction of streamflow using multiple proxies. Tree-ring data in South America has been used to reconstruct streamflow of major rivers in South America (Fernández et al., 2018; Ferrero et al., 2015; Holmes et al., 1979; Mundo et al., 2012; Muñoz et al., 2016), as well as drought conditions from 1400-present in the Southern Cone (Morales et al., 2020). The positive response of tree growth to ENSO variability shown here is influenced by the relationship between ENSO and

Table 3. Model statistics for reconstructions of the Tacuarembó and Negro Rivers in Uruguay.

	R.E	R^2	R^2adj	RMSEv	DW	Calibration period
TAC	0.33	0.456	0.399	58.74	1.87	1957–2009
NEG	0.28	0.407	0.344	364.27	1.85	1957–2009

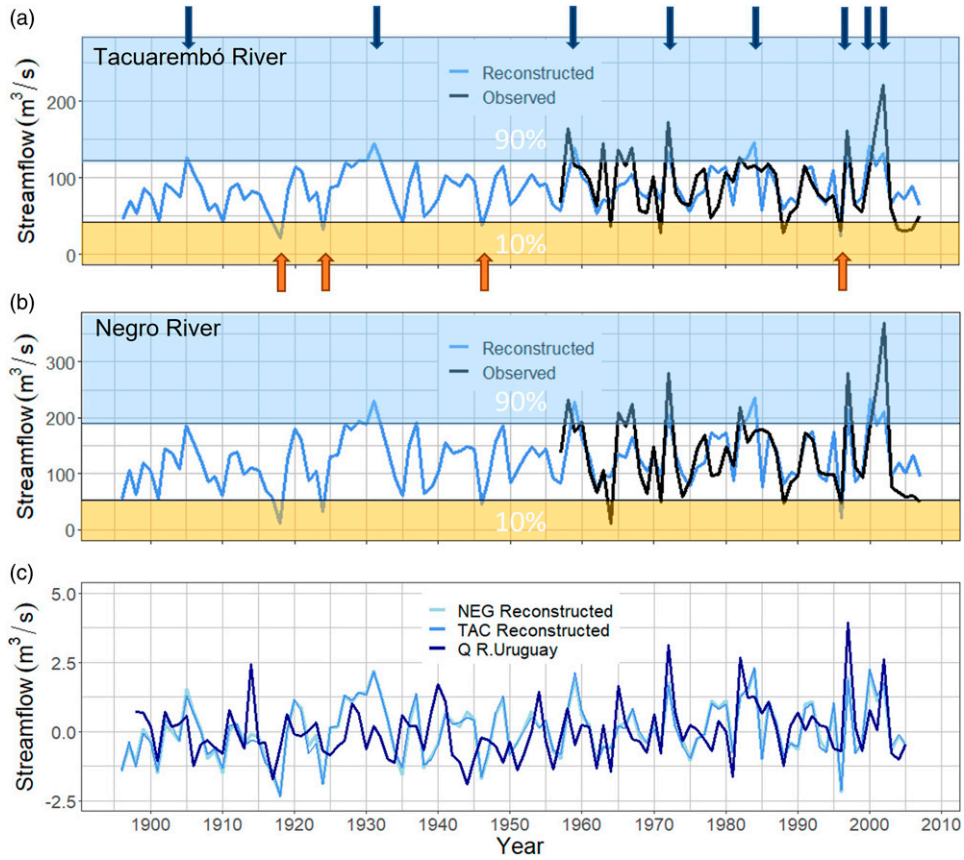

Figure 7. Reconstructed and observed annual Streamflow (Jun–May) of the (a) Tacuarembó River—Borracho Station and (b) Negro River—Mazangano Station in the Upper Negro River of Uruguay. Blue arrows indicate years >90% and in orange years <5% exceedance of annual Q. (c) The reconstructed annual Streamflow (Q, Jun–May) is compared to the Uruguay River at Concordia (CTM, 2020) from 1898 to 2005 (r = 0.40 for R. Tacuarembó and r = 0.38 for R. Negro). For interpretation of the references to colours in this figure legend, refer to the online version of this article.

local hydroclimate variables in both Central Chile and SESA (Garreaud et al., 2009). ENSO influences the interannual variability of annual tree growth of many chronologies in SA (Barichivich et al., 2009; Christie et al., 2009; Rigozo et al., 2004; Villalba, 1994). A positive correlation with the El Niño 3.4 Index was hypothesized as a potential mechanism for the positive correlation between annual growth in central Chile and Q in Uruguay. The months of the ENSO-tree-ring correlation in Chile varied

among species but generally coincided with the rainfall season in austral winter, prior to the onset of ring growth in the following September (Barichivich et al., 2009; Venegas-González et al., 2018). We found a positive correlation between the El Niño 3.4 Index during the austral winter-spring seasons and 16 of the 29 Central Chilean tree-ring chronologies. Radial growth increased during El Niño episodes, similar to findings in Mediterranean-temperate forests of Chile (Christie et al., 2009; Le Quesne et al., 2006; Venegas-González et al., 2018). Nonetheless, the correlation coefficient for the relationship between Chilean tree growth and Q was often higher than that of growth and ENSO, suggesting that other forcings besides ENSO mediate the hydroclimate teleconnection between Central Chile and Uruguay. Several studies in Chile have shown that the influence of ENSO on local hydroclimate varies by location and time scale (Barria et al., 2018; Muñoz et al., 2016; Rubio-Álvarez and McPhee, 2010). Six chronologies from different species contributed to the Q signal but did not correlate with ENSO (CAM, BLC, PYL, SAC, SVI, and PPI), potentially due to microclimatic and edaphic site conditions or tree species phenology. Among species, *Cryptocarya alba* (129-1002 masl) showed the highest correlations with Q, followed by *Kageneckia angustifolia* (2087-2100 masl), *Beilschmiedia miersii* (190-2000 masl), *Nothofagus macrocarpa* (1050-2000 masl), and *Austrocedrus chilensis* (1878 masl), among others, confirming the dendroclimatological potential of the Mediterranean tree species of Chile.

The ability of trees in Chile to track Q in Uruguay suggests that they are connected by multiple climate forcings including ENSO that deserve further research. The Southern Annual Mode (SAM), North Atlantic Oscillation (NAO) and Pacific Decadal Oscillation (PDO) all play a role in the inter-annual oscillations in Uruguay and Negro River Q (Maciel et al., 2013). SAM and Pacific Decadal Oscillation (PDO) are among other climate modes that influence annual growth in central Chile (Barichivich et al., 2009; Le Quesne et al., 2006; Venegas-González et al., 2018). Moreover, the ENSO signal in tree-rings varied over time, as shown here by the disconnect between ENSO and the 100-year composite chronology in 1940 to 1980. The ENSO signal in other Chilean chronologies is also modular, with a strong influence at the onset of the 20th century (Rigozo et al., 2004). If ENSO is one of multiple climate forcings that connect rainfall in central Chile and SESA (Barria et al., 2018; Muñoz et al., 2016; Rubio-Álvarez and McPhee, 2010), then we could expect tree-rings to track Q despite this time-dependent correlation with ENSO.

Tree-rings in Uruguay and Central Chile were related to hydroclimate in different seasons. Due to seasonal rainfall in Chile, chronologies and the reconstruction were more strongly correlated with Q in winter-early spring months. Meanwhile, year-round rainfall patterns and hot summers in Uruguay explain the strong correlation with Q in summer-fall months. Late summer—early fall is a critical period for water supply in these agricultural watersheds of NE Uruguay, where 87% of the freshwater supply used in the country is destined for irrigation (MVOTMA, 2017). High rates of evapotranspiration and evaporation during the summer months of Dec–Feb have a major influence over water availability downstream for agriculture and power generation (Jobbagy et al., 2011). Droughts during these months affect not only water supply for agriculture, silviculture, and power generation but also facilitate low-flow conditions for the development of algal blooms (Haakonsson et al., 2017).

4.2 Reconstructed streamflow of rivers in Uruguay

Reconstructed Q of the two major tributaries of the Upper Negro River basin highlights interannual variability of two major rivers in northeastern Uruguay over the past century, surpassing the instrumental period by over 60 years. The 115-year reconstruction confirms observed trends among the few long-term instrumental records in the region of increasing extreme flood events over time, related to the "climatic jump" of increasing precipitation and Q since the 1960s (Mechoso and Iribarren, 1992). Similarly, the Uruguay River displays a 40% increase in annual Q post-1970s, related to an increase in precipitation in ENSO-neutral months (*e.g.,* Jan–Feb), and not to the increase in the number of El Niño months post-1970s (Doyle and Barros, 2011). The reconstruction captured high-flow years of > 90% during 1905, 1929, 1931–1932, and 1958–1959, a year that included the largest flooding event on record in April 1959 in the

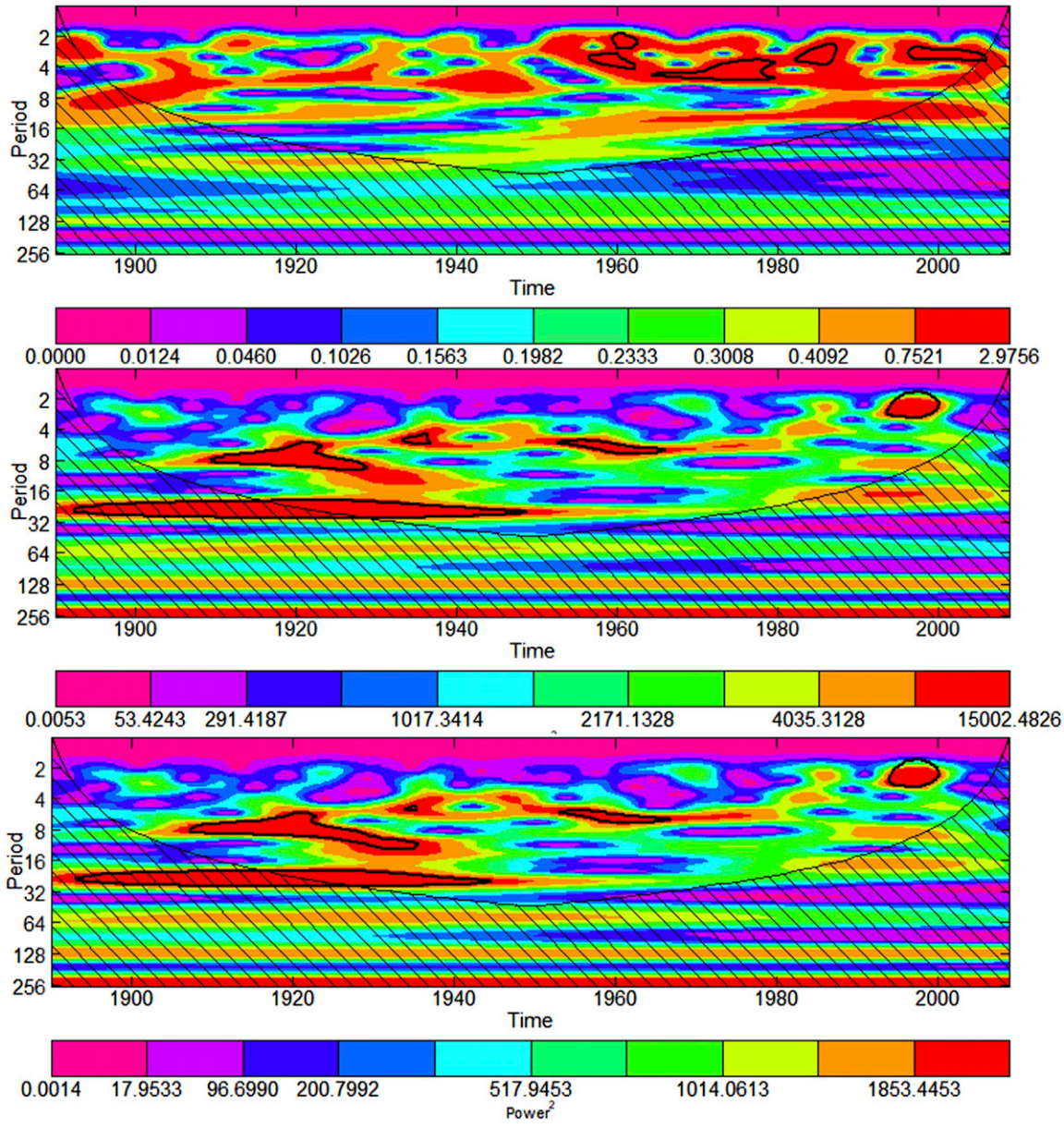

Figure 8. Wavelet plots showing periodicity of (a) reconstructed Q for the Tacuarembo River, (b) reconstructed Q for the Negro River, and (c) ENSO (averaged over Aug–Dec) El Nino 3.4 Index during the reconstructed time period 1890–2009. Black outlines indicate significance. For interpretation of the references to colours in this figure legend, refer to the online version of this article.

Negro River basin. Many of these years coincide with El Niño periods in the historical record. Nonetheless, the lack of strong 2–7 year periodicity throughout the reconstruction suggests that ENSO may be one of many climate drivers for Q variability in SESA, influencing cycles of longer periodicity of 8–30 years. The high frequency of high-flow events in the latter part of the century is concurrent with the predicted

increase in the frequency of 100-year floods in the twenty-first century (Hirabayashi et al., 2013) and a decrease in water shortage events (Krepper and Zucarelli, 2010). The reconstructions also captured low-flow years of <10% exceedance in 1890, 1917–1918, 1924, 1946, and 1996, highlighting the decreased frequency of low-flow events in the second half of the century. Although the Uruguay River basin extends 300,000 km^2 5%, the historical hydrometric data from Concepcion since 1898 confirms the reconstructed variability in Q of these smaller interior basins, suggesting that the Tacuarembo and Negro respond to regional climate signals in SESA.

The reliability of reconstructed Q is potentially affected by both recent climate phenomena in Chile and land-use change in Uruguay. The reconstructed Q was terminated in 2009 despite available reconstructed values through 2017, due to a decoupling of Chilean tree ring growth and Negro River Q in the last decade. This was also confirmed by changes in the double mass curve between Central Chile and NE Uruguay precipitation, which until approximately 2000 was consistent from 1901 to 1999. The severe decline in annual growth in the last two decades of trees in Central Chile coincides with the megadrought in the region in the last two decades (Boisier et al., 2016; Garreaud et al., 2020). The recent conversion of grasslands to afforestation in SESA (Cespedes-Payret et al., 2009; Silveira et al., 2016) could also confound the relationship between tree-rings and Q in future decades (Arriaga, 2018). The increase in *Eucalyptus* spp. plantation area in the study region since 2000 is associated with a decline in annual Q of 17–35% and a seasonal decline in spring-summer Q of 25–38% in the Tacuarembó River—Borracho hydrometric station (Silveira and Alonso, 2009). An estimated 53% of the Tacuarembó River basin is designated as "priority soils" for development of tree plantation forestry, and plans exist for a new cellulose plant on the Negro River with a projected annual production rate of 1.9–2.4 million tons of cellulose pulp (UPM - ROU Agreement, 2019). Management of water resources will need to evaluate the combined effects of increasing rainfall and flooding events as shown by the IPCC (2021), with changes in water balance due to land cover change (Brown et al., 2005).

Reconstructed Q provides a necessary long-term perspective on changes in water availability over multiple decades. Changes in how instrumental Q is estimated, periods of missing data, riverbed changes over time due to natural processes of erosion and deposition, and uncertainty regarding gauging curve development and maintenance all potentially contribute to errors within the instrumental data, particularly prior to the 1980s. Current legislation in Uruguay regarding water management for irrigation—to which more than 80% of water used in Uruguay is designated—requires 20 years of monthly Q to determine environmental streamflow (*Ley de Riego*—Decree 366/018). Despite the potential errors in historical data, this study shows that 20-year time windows poorly capture the long-term variability in streamflow, including mean summer flow, frequency and severity of drought and flood events (Razavi et al., 2015). The 115-year reconstruction suggests major flooding events in 1930, 1959, 1966, and 1998, all of which could be potentially excluded from an estimation of environmental streamflow in the last two decades. In Chile, dendrohydrological reconstructions using tree-rings show that Q during the period used to legally determine water allocation was above the long-term mean (Fernández et al., 2018). As central Chile currently faces severe drought and a decline in tree growth in the past two decades (Garreaud et al., 2020; Miranda et al., 2020; Venegas-González et al., 2019), the allocation of water based on a surplus of discharge has had severe ecological and economic consequences. Sustainable water management under future land-use and climate scenarios will rely in part on historical Q data to develop sound predictions regarding water availability and flood risk.

V Conclusions

We suggest that, in addition to the reconstruction of drought atlas that networks of tree-ring chronologies from Southern South America provide a regional proxy for annual streamflow for rivers in the grassland-dominated agricultural regions of Southeastern South America. This connection between Central Chilean tree growth and Negro River Q in Uruguay was mediated by the influence of ENSO and, likely by other regional climate phenomena that merit further research. Given

the context of water management in the Negro River basin as climate and land-cover change this grassland-dominated landscape, a proxy for historical streamflow lends insight into river oscillations over multiple decades. Nonetheless, changing land-use patterns, the modular behavior of the ENSO-regional climate relationship, and human impacts on river hydrology could all confound the reliability of distant long-term chronologies to predict annual river discharge.

Given the scarcity of forest ecosystems and long-lived trees in SESA, the extensive network of tree-ring chronologies from higher elevations of the Pacific coastal ranges of South America have a large potential to reconstruct long-term hydroclimate in much of Southern South America (Morales et al., 2020). While tree-ring chronologies from the Negro River basin in Uruguay tracked seasonal hydrological drought and annual Q variability, long-term tree-ring chronologies from Chile filled in major decadal gaps in historical hydrological variability, thus improving reconstructions of annual Q in this agricultural epicenter of South America. Overall, this study highlights how tree-ring networks in South America can contribute to understanding seasonal and annual variation in hydrological regimes in data-poor regions. In the context of the increasing frequency of severe flooding events in SESA, hydroclimatological proxies from forest ecosystems can extend the historical record as a reference for future decisions regarding water use and management, within the context of climate change and land-use transformation.

Declaration of conflicting interests

The author(s) declared no potential conflicts of interest with respect to the research, authorship and/or publication of this article

Funding

The author(s) disclosed receipt of the following financial support for the research, authorship, and/or publication of this article: This article was supported by Research Nucleus in Nature Based Solutions (PUCV 039.431/2020); Center for Climate Action (PUCV ESR UCV2095); Chilean Research Council (REDES N°180187); Agencia Nacional de Investigación e Innovación (FCE_1_2019_1_155963, PD_NAC_2012_1_7627); Center for Climate and Resilience Research (ANID, FONDAP N°15110009); Comisión Sectorial de Investigación Científica (NA); Agencia Nacional de Investigación y Desarrollo (Subdirección de Capital Humano/Doctorado Nacional); Fondo Nacional de Desarrollo Científico y Tecnológico (1201714); Agencia Nacional de Investigacion y Desarollo (ANID) (FONDECYT N°11180992).

ORCID iDs

Christine Lucas https://orcid.org/0000-0003-2460-1516
Isabella Aguilera-Betti https://orcid.org/0000-0001-5052-6033
Paulina Puchi https://orcid.org/0000-0001-5429-8605

Supplemental Material

Supplemental material for this article is available online.

References

Aguilera-Betti I, Muñoz AA, Stahle D, et al. (2017) The first millennium-age Araucaria araucana in Patagonia. *Tree-Ring Research* 73: 53–56.

Allan RJ (1988) El Niño southern oscillation influences in the Australasian region. *Progress in Physical Geography* 12: 313–348.

Allen EB, Rittenour TM, DeRose RJ, et al. (2013) A tree-ring based reconstruction of Logan River streamflow, northern Utah. *Water Resources Research* 49: 8579–8588.

Arriaga ME (2018) *Resultados de la Cartografía Forestal Nacional 2018*. Montevideo: Dirección General Forestal - Ministerio de Ganadería Agricultura y Pesca. https://www.gub.uy/ministerio-ganaderia-agricultura-pesca/datos-y-estadisticas/datos/resultados-cartografia-forestal-nacional-2018.

Baldi G and Paruelo JM (2008) Land-use and land cover dynamics in South American temperate grasslands. *Ecology and Society* 13(2): 6.

Barichivich J, Sauchyn DJ and Lara A (2009) Climate signals in high elevation tree-rings from the semiarid Andes of north-central Chile: responses to regional and large-scale variability. *Palaeogeography, Palaeoclimatology, Palaeoecology* 281: 320–333.

Barria P, Peel MC, Walsh KJ, et al. (2018) The first 300-year streamflow reconstruction of a high-elevation river in Chile using tree rings. *International Journal of Climatology* 38: 436–451.

Barros V, Doyle M and Camilloni I (2005) Potential impacts of climate change in the Plata basin. In: *Regional Hydrological Impacts of Climate Change: Impact Assessment and Decision Making*. China: IAHS.

Biondi F and Waikul K (2004) DENDROCLIM2002: a C++ program for statistical calibration of climate signals in tree-ring chronologies. *Computers & Geosciences* 30: 303–311.

Blasing T, Solomon A and Duvick D (1984) Response functions revisited. *Tree-Ring Bulletin* 44: 1–15.

Bogino SM and Jobbágy EG (2011) Climate and groundwater effects on the establishment, growth and death of Prosopis caldenia trees in the Pampas (Argentina). *Forest Ecology and Management* 262: 1766–1774.

Boisier JP, Rondanelli R, Garreaud RD, et al. (2016) Anthropogenic and natural contributions to the Southeast Pacific precipitation decline and recent megadrought in central Chile. *Geophysical Research Letters* 43: 413–421.

Bond N (2018) *Hydrostats: Hydrologic Indices for Daily Time Series Data*. v. 0.2. 6. Relived from: https://github.com/nickb.ond/hydro.stats.

Briffa KR (1995) Interpreting high-resolution proxy climate data—the example of dendroclimatology. In: von Storch H and Navarra A (eds) *Analysis of Climate Variability*. Berlin, Heidelberg, New York: Springer, 77–94.

Brown AE, Zhang L, McMahon TA, et al. (2005) A review of paired catchment studies for determining changes in water yield resulting from alterations in vegetation. *Journal of Hydrology* 310: 28–61.

Bunn AG (2008) A dendrochronology program library in R (dplR). *Dendrochronologia* 26: 115–124.

Camilloni IA, Saurral RI and Montroull NB (2013) Hydrological projections of fluvial floods in the Uruguay and Paraná basins under different climate change scenarios. *International Journal of River Basin Management* 11: 389–399.

Cavalcanti I, Carril A, Penalba O, et al. (2015) Precipitation extremes over La Plata Basin–Review and new results from observations and climate simulations. *Journal of Hydrology* 523: 211–230.

Cazes-Boezio G, Robertson AW and Mechoso CR (2003) Seasonal dependence of ENSO teleconnections over South America and relationships with precipitation in Uruguay. *Journal of Climate* 16: 1159–1176.

Cespedes-Payret C, Piñeiro G, Achkar M, et al. (2009) The irruption of new agro-industrial technologies in Uruguay and their environmental impacts on soil, water supply and biodiversity: a review. *International Journal of Environment and Health* 3: 175–197.

Chiew FH and McMahon TA (2002) Global ENSO-streamflow teleconnection, streamflow forecasting and interannual variability. *Hydrological Sciences Journal* 47: 505–522.

Christie DA, Boninsegna JA, Cleaveland MK, et al. (2011) Aridity changes in the temperate-mediterranean transition of the Andes since AD 1346 reconstructed from tree-rings. *Climate Dynamics* 36: 1505–1521.

Christie DA, Lara A, Barichivich J, et al. (2009) El Niño-Southern Oscillation signal in the world's highest-elevation tree-ring chronologies from the Altiplano, Central Andes. *Palaeogeography, Palaeoclimatology, Palaeoecology* 281: 309–319.

Coulthard BL, Anchukaitis KJ, Pederson GT, et al. (2021) Snowpack signals in North American tree rings. *Environmental Research Letters* 16: 034037.

CTM (2020) *Streamflow data from 1898-2005 for the Concordia hydrometric station of the Uruguay River*. [Unpublished raw data]. Comisión Técnica Mixta (CTM) de Salto Grande (Uruguay-Argentina).

Cuya DGP, Brandimarte L, Popescu I, et al. (2013) A GIS-based assessment of maximum potential hydropower production in La Plata basin under global changes. *Renewable Energy* 50: 103–114.

DINAGUA (2018) *Monthly time series for streamflow of rivers in the Negro River Basin,* Uruguay [Unpublished raw data]. Dirección Nacional de Agua (DINAGUA) - Ministerio de Ambiente, Uruguay.

Doyle ME and Barros VR (2011) Attribution of the river flow growth in the Plata Basin. *International Journal of Climatology* 31: 2234–2248.

Fernández A, Muñoz A, González-Reyes Á, et al. (2018) Dendrohydrology and water resources management in south-central Chile: lessons from the Río Imperial streamflow reconstruction. *Hydrology and Earth System Sciences* 22: 2921–2935.

Ferrero ME, Villalba R, De Membiela M, et al. (2015) Tree-ring based reconstruction of Río Bermejo streamflow in subtropical South America. *Journal of Hydrology* 525: 572–584.

Fritts H (1976) *Tree Rings and Climate*. New York: Academic Press.

Gallant AJ and Gergis J (2011) An experimental streamflow reconstruction for the River Murray, Australia, 1783–1988. *Water Resources Research* 47(12): W00G04.

García NO and Vargas WM (1998) The temporal climatic variability in the 'Río de la Plata'basin displayed by the river discharges. *Climatic Change* 38: 359–379.

Garreaud R (2009) The Andes climate and weather. *Advances in Geosciences* 22: 3–11.

Garreaud RD, Alvarez-Garreton C, Barichivich J, et al. (2017) The 2010–2015 megadrought in central Chile: impacts on regional hydroclimate and vegetation. *Hydrology and Earth System Sciences* 21: 6307–6327.

Garreaud RD, Boisier JP, Rondanelli R, et al. (2020) The central Chile mega drought (2010–2018): a climate dynamics perspective. *International Journal of Climatology* 40: 421–439.

Garreaud RD, Vuille M, Compagnucci R, et al. (2009) Present-day south american climate. *Palaeogeography, Palaeoclimatology, Palaeoecology* 281: 180–195.

Genta J, Perez-Iribarren G and Mechoso CR (1998) A recent increasing trend in the streamflow of rivers in southeastern South America. *Journal of Climate* 11: 2858–2862.

Grimm AM, Barros VR and Doyle ME (2000) Climate variability in southern South America associated with El Niño and La Niña events. *Journal of Climate* 13: 35–58.

Grimm AM and Tedeschi RG (2009) ENSO and extreme rainfall events in South America. *Journal of Climate* 22: 1589–1609.

Haakonsson S, Rodríguez-Gallego L, Somma A, et al. (2017) Temperature and precipitation shape the distribution of harmful cyanobacteria in subtropical lotic and lentic ecosystems. *Science of the Total Environment* 609: 1132–1139.

Harris I, Osborn TJ, Jones P, et al. (2020) Version 4 of the CRU TS monthly high-resolution gridded multivariate climate dataset. *Scientific Data* 7: 109.

Higgins P, Palmer J, Turney C, et al. (2020) One thousand three hundred years of variability in the position of the South Pacific convergence zone. *Geophysical Research Letters* 47: e2020GL088238.

Hirabayashi Y, Mahendran R, Koirala S, et al. (2013) Global flood risk under climate change. *Nature Climate Change* 3: 816–821.

Holmes R, Stockton C and LaMarche V Jr (1979) Extension of river flow records in Argentina from long tree-ring chronologies. *JAWRA Journal of the American Water Resources Association* 15: 1081–1085.

Holmes RL (1983) *Program COFECHA User's Manual*. Tucson: Laboratory of Tree-Ring Research, The University of Arizona.

IPCC (2014) Climate Change 2014: Impacts, adaptation, and vulnerability. part a: global and sectoral aspects. *Contribution of Working Group II to the Fifth Assessment Report of the Intergovernmental Panel on Climate Change*. Field CB, Barros VR, Dokken DJ, et al. (eds). Cambridge University Press, Cambridge, UK and New York, NY, USA: IPCC, pp. 1132.

IPCC (2021) *Climate Change 2021: The Physical Science Basis. Contribution of Working Group I to the Sixth Assessment Report of the Intergovernmental Panel on Climate Change*. Masson-Delmotte V, Zhai P, Pirani A, et al. (eds). Cambridge University Press. In Press.

Jobbagy EG, Nosetto MD, Villagra PE, et al. (2011) Water subsidies from mountains to deserts: their role in sustaining groundwater-fed oases in a sandy landscape. *Ecological Applications* 21: 678–694.

Krepper C, García N and Jones P (2003) Interannual variability in the Uruguay river basin. *International Journal of Climatology: A Journal of the Royal Meteorological Society* 23: 103–115.

Krepper CM and Zucarelli GV (2010) Climatology of water excesses and shortages in the La Plata Basin. *Theoretical and Applied Climatology* 102: 13–27.

Lara A, Villalba R, Urrutia-Jalabert R, et al. (2020) + A 5680-year tree-ring temperature record for southern South America. *Quaternary Science Reviews* 228: 106087.

Le Quesne C, Acuña C, Boninsegna JA, et al. (2009) Long-term glacier variations in the Central Andes of Argentina and Chile, inferred from historical records and tree-ring reconstructed precipitation. *Palaeogeography, Palaeoclimatology, Palaeoecology* 281: 334–344.

Le Quesne C, Stahle DW, Cleaveland MK, et al. (2006) Ancient Austrocedrus tree-ring chronologies used to reconstruct central Chile precipitation variability from AD 1200 to 2000. *Journal of Climate* 19: 5731–5744.

Lee SJ and Berbery EH (2012) Land cover change effects on the climate of the La Plata basin. *Journal of Hydrometeorology* 13(1): 84–102.

Lehner B, Verdin K and Jarvis A (2008) New global hydrography derived from spaceborne elevation data.

Eos, Transactions American Geophysical Union 89: 93–34.

Lucas C, Puchi P, Profumo L, et al. (2018) Effect of climate on tree growth in the Pampa biome of Southeastern South America: first tree-ring chronologies from Uruguay. *Dendrochronologia* 52: 113–122.

Maciel F, Díaz A and Terra R (2013) Multi-annual variability of streamflow in La Plata Basin. Part I: observations and links to global climate. *International Journal of River Basin Management* 11: 345–360.

Matskovsky V, Venegas-González A, Garreaud R, et al. (2021) Tree growth decline as a response to projected climate change in the 21st century in mediterranean mountain forests of Chile. *Global and Planetary Change* 198: 103406.

Marshall GJ, (2003) Trends in the Southern Annular Mode from observations and reanalyses. *Journal of Climate* 16: 4134-4143

Maxwell RS, Harley GL, Maxwell JT, et al. (2017) An interbasin comparison of tree-ring reconstructed streamflow in the eastern United States. *Hydrological Processes* 31: 2381–2394.

Mechoso CR, Dıas P, Baetghen W, et al. (2001) Climatology and hydrology of the La Plata Basin. Document of VAMOS/CLIVAR document, 55. https://www.clivar.org/sites/default/files/documents/vamos/laplata.pdf.

Mechoso CR and Iribarren GP (1992) Streamflow in southeastern South America and the southern oscillation. *Journal of Climate* 5: 1535–1539.

Meko DM and Woodhouse CA (2011) Application of streamflow reconstruction to water resources management. In: *Dendroclimatology*. Berlin, Heidelberg, New York: Springer, 231–261.

Meza FJ (2013) Recent trends and ENSO influence on droughts in Northern Chile: an application of the Standardized Precipitation Evapotranspiration Index. *Weather and Climate Extremes* 1: 51–58.

Michaelsen J (1987) Cross-validation in statistical climate forecast models. *Journal of Applied Meteorology and Climatology* 26: 1589–1600.

Miranda A, Lara A, Altamirano A, et al. (2020) Forest browning trends in response to drought in a highly threatened mediterranean landscape of South America. *Ecological Indicators* 115: 106401.

Modernel P, Rossing WA, Corbeels M, et al. (2016) Land use change and ecosystem service provision in Pampas and Campos grasslands of southern South America. *Environmental Research Letters* 11(11): 113002.

Montecinos A and Aceituno P (2003) Seasonality of the ENSO-related rainfall variability in central Chile and associated circulation anomalies. *Journal of Climate* 16: 281–296.

Morales MS, Cook ER, Barichivich J, et al. (2020) Six hundred years of South American tree rings reveal an increase in severe hydroclimatic events since mid-20th century. *Proceedings of the National Academy of Sciences* 117: 16816–16823.

Mundo IA, Masiokas MH, Villalba R, et al. (2012) Multi-century tree-ring based reconstruction of the Neuquén River streamflow, northern Patagonia, Argentina. *Climate of the Past* 8: 815–829.

Muñoz AA, González-Reyes A, Lara A, et al. (2016) Streamflow variability in the Chilean Temperate-Mediterranean climate transition (35 S–42 S) during the last 400 years inferred from tree-ring records. *Climate Dynamics* 47: 4051–4066.

Muñoz AA, Klock-Barría K, Alvarez-Garreton C, et al. (2020) Water crisis in Petorca Basin, Chile: The combined effects of a mega-drought and water management. *Water* 12: 648.

MVOTMA (2017) *Plan Nacional de Aguas*. Montevideo: MVOTMA. http://www.mvotma.gub.uy/politica-nacional-de-aguas/plan-nacional-de-aguas.

Oliveira JM, Roig FA and Pillar VD (2010) Climatic signals in tree-rings of Araucaria angustifolia in the southern Brazilian highlands. *Austral Ecology* 35: 134–147.

Pasquini AI and Depetris PJ (2007) Discharge trends and flow dynamics of South American rivers draining the southern Atlantic seaboard: an overview. *Journal of Hydrology* 333: 385–399.

Penalba OC and Rivera JA (2016) Precipitation response to El Niño/La Niña events in Southern South America–emphasis in regional drought occurrences. *Advances in Geosciences* 42: 1–14.

Pisciottano G, Díaz A, Cazess G, et al. (1994) El niño-southern oscillation impact on rainfall in Uruguay. *Journal of Climate* 7: 1286–1302.

R Core Team (2019) *R: A Language and Environment for Statistical Computing*. Vienna, Austria: R Foundation for Statistical Computing. https://www.R-project.org/.

Razavi S, Elshorbagy A, Wheater H, et al. (2015) Toward understanding nonstationarity in climate and

hydrology through tree ring proxy records. *Water Resources Research* 51: 1813–1830.

Rigozo NR, Nordemann DJ, Echer E, et al. (2004) ENSO influence on tree ring data from Chile and Brazil. *Geofísica Internacional* 43: 287–294.

Robertson AW and Mechoso CR (1998) Interannual and decadal cycles in river flows of southeastern South America. *Journal of Climate* 11: 2570–2581.

Rubel F and Kottek M (2010) Observed and projected climate shifts 1901-2100 depicted by world maps of the Köppen-Geiger climate classification. *Meteorologische Zeitschrift* 19: 135.

Rubio-Álvarez E and McPhee J (2010) Patterns of spatial and temporal variability in streamflow records in south central Chile in the period 1952–2003. *Water Resources Research* 46: W05514.

Sauchyn D, Vanstone J and Perez-Valdivia C (2011) Modes and forcing of hydroclimatic variability in the Upper North Saskatchewan River Basin since 1063. *Canadian Water Resources Journal/Revue canadienne des ressources hydriques* 36: 205–217.

Schneider DP, Deser C, Fasullo J, et al. (2013) Climate data guide spurs discovery and understanding. *Eos, Transactions American Geophysical Union* 94: 121–122.

Silveira L and Alonso J (2009) Runoff modifications due to the conversion of natural grasslands to forests in a large basin in Uruguay. *Hydrological Processes: An International Journal* 23: 320–329.

Silveira L, Gamazo P, Alonso J, et al. (2016) Effects of afforestation on groundwater recharge and water budgets in the western region of Uruguay. *Hydrological Processes* 30: 3596–3608.

Speer JH (2010) *Fundamentals of Tree-Ring Research*. Tucson, AZ, USA: University of Arizona Press.

Talento S and Terra R (2013) Basis for a streamflow forecasting system to Rincón del Bonete and Salto Grande (Uruguay). *Theoretical and Applied Climatology* 114: 73–93.

Tencaliec P, Favre AC, Prieur C, et al. (2015) Reconstruction of missing daily streamflow data using dynamic regression models. *Water Resources Research* 51: 9447–9463.

Toranza C, Lucas C and Ceroni M (2019) Spatial distribution and tree cover of hillside and ravine forests in Uruguay: the challenges of mapping patchy ecosystems. *Agrociencia (Montevideo)* 23: 135–146.

Trenberth KE (1997) The definition of el Niño. *Bulletin of the American Meteorological Society* 78: 2771–2778.

Trouet V and Van Oldenborgh GJ (2013) KNMI climate explorer: a web-based research tool for high-resolution paleoclimatology. *Tree-Ring Research* 69: 3–13.

ROU - UPM Agreement (2017) *Agreement between the Republic of Uruguay (ROU) and UPM Pulp OY* [unpublished document].

Vega E, Baldi G, Jobbágy EG, et al. (2009) Land use change patterns in the Río de la Plata grasslands: the influence of phytogeographic and political boundaries. *Agriculture, Ecosystems & Environment* 134: 287–292.

Venegas-González A, Juñent FR, Gutiérrez AG, et al. (2018) Recent radial growth decline in response to increased drought conditions in the northernmost Nothofagus populations from South America. *Forest Ecology and Management* 409: 94–104.

Venegas-González A, Roig FA, Peña-Rojas K, et al. (2019) Recent consequences of climate change have affected tree growth in distinct Nothofagus macrocarpa (DC.) FM Vaz & Rodr age classes in Central Chile. *Forests* 10: 653.

Vicente-Serrano SM, Beguería S and López-Moreno JI (2010) A multiscalar drought index sensitive to global warming: the standardized precipitation evapotranspiration index. *Journal of Climate* 23: 1696–1718.

Villalba R (1994) Tree-ring and glacial evidence for the Medieval Warm Epoch and the Little Ice Age in southern South America. In: *The Medieval Warm Period.* Berlin, Heidelberg, New York: Springer, 183–197.

Villalba R, Lara A, Masiokas MH, et al. (2012) Unusual Southern Hemisphere tree growth patterns induced by changes in the Southern annular mode. *Nature Geoscience* 5: 793–798.

Williams A, Anchukaitis K, Woodhouse C, et al. (2021) Tree rings and observations suggest no stable cycles in Sierra Nevada cool-season precipitation. *Water Resources Research* 57: e2020WR028599.

Zang C and Biondi F (2015) treeclim: an R package for the numerical calibration of proxy-climate relationships. *Ecography* 38: 431–436.

View publication stats